Stokes-correlometric differentiation of polarization-heterogeneous images of biological tissues and some legal aspects of the use of early diagnosis of diseases

A. Dubolazov, N. Getmantseva, A. Getmantsev, Yu. Ushenko, M. Gorsky, et al.

A. V. Dubolazov, N. D. Getmantseva, A. V. Getmantsev, Yu. O. Ushenko, M. P. Gorsky, M. M. Slyotov, V. G. Zhytaryuk, N. P. Penteleichuk, "Stokes-correlometric differentiation of polarization-heterogeneous images of biological tissues and some legal aspects of the use of early diagnosis of diseases," Proc. SPIE 11369, Fourteenth International Conference on Correlation Optics, 113691W (6 February 2020); doi: 10.1117/12.2553975

SPIE.

Event: Fourteenth International Conference on Correlation Optics, 2019, Chernivtsi, Ukraine

Stokes-correlometric differentiation of polarization-heterogeneous images of biological tissues and some legal aspects of the use of early diagnosis of diseases

A.V. Dubolazov[1], N. D. Getmantseva[1], A. V.Getmantsev[1], Yu.O. Ushenko[1], M.P. Gorsky[1], M.M. Slyotov[1], V.G. Zhytaryuk[1], N. P. Penteleichuk[2]

[1]Chernivtsi National University, 2 Kotsiubynskyi Str., Chernivtsi, Ukraine, 58012
[2] Bukovinian State Medical University, 3 Theatral Sq., Chernivtsi, Ukraine, 58000

a.dubolazov@chnu.edu.ua

ABSTRACT

This research contains the results:
1. of the method of Stokes-correlometric mapping, the physical processes of changes in optical anisotropy (distribution of optical axis directions and phase modulation) of biological structured (kidney) and parenchymal (liver) tissues of rat internal organs, which are caused by systemic pathology (diabetes), were identified and analyzed as part of a statistical analysis.
2. of the most sensitive parameters (statistical moments of the 1st – 4th orders of magnitude, the correlation moment of the 4th order) to changes in the distribution structure of the magnitude and phase of the SCS of the 3rd and 4th parameters of the "two-point" parameter of the Stokes polarization heterogeneous microscopic images of histological sections of healthy and diabetic rat kidney and liver tissues.
3. of social and legal aspects of implementation of methods for early diagnosis of systemic diseases in public society.

Keywords: Stokes-correlometry, wavelet analysis, spatial-frequency filtering, biological tissues

1. Introduction

In a series of scientific papers [1-12], the possibility of polarimetric differentiation of fibrillar biological tissue samples of healthy and sick people was demonstrated. At the same time, a high sensitivity of laser polarimetry methods is achieved, which is determined by a significant difference in the average (within the control and studied groups of biological layers) values of statistical moments characterizing the distribution of polarization parameters (azimuth and polarization ellipticity) of a series of microscopic images. At the same time, most of the vital organs of the person (liver, stomach, pancreas, spleen, lungs, etc.) have a different parenchymal structure. Here optically anisotropic formations are formed in the form of separate, spatially localized "islands". Due to this change in birefringence as a result of pathological disordering, the directions of the optical axes are smaller. Therefore, statistical analysis in these cases is less effective.
The objective of this work is to generalize the polarization-correlation description of the optical manifestations of the phase anisotropy of polycrystalline networks using the "two-point" vector-parametric approach and to develop new methods for multiparameter mapping of the degree of correlation of the module and phase of the parameters of the Stokes vector of polarization-inhomogeneous images of biological layers[13-17].

2. Model approach

It is shown that for laser radiation with a wavelength $\lambda = 0.63\mu m$ within the geometric thickness $l = 30\mu m$ of the completely optically anisotropic layer of biological tissue ($\Delta n \approx 10^{-4} \div 1.5 \times 10^{-3}$)[2,7,8], the maximum phase shift ($\delta_{12} \equiv \delta = \frac{2\pi}{\lambda}\Delta nl$) varies widely $0.03 \le \delta \le 0.45$. Among birefringent networks or "islands", there are variations in

Fourteenth International Conference on Correlation Optics, edited by Oleg V. Angelsky, Proc. of SPIE Vol. 11369, 113691W · © 2020 SPIE
CCC code: 0277-786X/20/$21 · doi: 10.1117/12.2553975

transverse dimensions ($2\mu m \le \Delta l \le 20\mu m$), which form weak phase modulations in the plane of a polarization-inhomogeneous image.

Under these conditions, the expressions for the module ($|\ |$) and phase (Arg) of the two-point parameters of the Stokes vector (SCS) take the following form

$$\begin{cases} |S_1| = [1 + tg\rho_1 tg\rho_2]; \\ ArgS_1 = arctg\left[\dfrac{(\delta_2 - \delta_1)}{1 + ctg\rho_1 ctg\rho_2}\right]. \end{cases} \begin{cases} |S_2| = [1 - tg\rho_1 tg\rho_2]; \\ ArgS_2 = arctg\left[\dfrac{(\delta_2 - \delta_1)}{ctg\rho_1 ctg\rho_2}\right]. \end{cases} \begin{cases} |S_3| = 1 - ctg\rho_2 tg\rho_1; \\ ArgS_3 = arctg\left(\dfrac{\delta_2 - \delta_1 ctg\rho_2 tg\rho_1}{1 + ctg\rho_2 tg\rho_1}\right); \end{cases}$$

$$\begin{cases} |S_4| = 1 + ctg\rho_2 tg\rho_1; \\ ArgS_4 = arctg\left(\dfrac{1 + ctg\rho_2 tg\rho_1}{\delta_1 + \delta_2 ctg\rho_2 tg\rho_1}\right). \end{cases} \quad (1)$$

From (1) it follows that the SCS module $\left|S_{i=1;2;3;4}(\Delta x, \Delta y)\right|$ carries information on the orientational structure (direction of the optical axis $\rho(x, y)$) of polycrystalline networks and structures. The SCS phase $Arg\left(S_{i=1;2;3;4}(\Delta x, \Delta y)\right)$ carries information about their birefringence (phase shift - $\delta(x, y)$).

3. The methodology for measuring the coordinate distributions of the module and the SCS phase of the object field of the biological layer

The experimental technique of Stokes-correlometric mapping of the object field of a biological layer consists in the following sequence of steps[18-20]:

1. The sample is irradiated with a circularly polarized laser beam.

2. Rotate the axis of transmission of the polarizer-analyzer (in the absence of a quarter-wave plate) by the angles $\Theta = 0^0$, $\Theta = 90^0$, $\Theta = 45^0$, $\Theta = 135^0$ and measure the intensity of the transmitted radiation $I_0^{\otimes}; I_{90}^{\otimes}; I_{45}^{\otimes}; I_{135}^{\otimes}$.

3. The value of the first, second and third parameters of the Stokes vector $S_{i=1;2;3}^{\otimes}$ is calculated within each pixel of the digital camera

$$S_1 = I_0^{\otimes} + I_{90}^{\otimes}; S_2 = I_0^{\otimes} - I_{90}^{\otimes};\ S_3 = I_{45}^{\otimes} - I_{135}^{\otimes}. \quad (2)$$

4. Install a quarter-wave plate in front of the polarizer-analyzer, orient its axis of maximum speed at angles $+45^0$ and -45^0 relative to the plane of transmission of the polarizer, and measure the intensity of the transmitted radiation $I_{\otimes}^{\otimes}; I_{\oplus}^{\otimes}$.

5. Calculate a two-dimensional array of values of the fourth parameter of the Stokes vector S_4 .

$$S_4 = I_{\otimes}^{\otimes} - I_{\oplus}^{\otimes}. \quad (3)$$

6. The coordinate distributions of the values of the two-point parameters of the Stokes vector are calculated by the following algorithms:

$$\begin{cases} |S_2| = \sqrt{\left[\sqrt{I_0(r_1)I_0(r_2)} - \sqrt{I_{90}(r_1)I_{90}(r_2)}\cos(\delta_2 - \delta_1)\right]^2 + \left[\sqrt{I_{90}(r_1)I_{90}(r_2)}\sin(\delta_2 - \delta_1)\right]^2}; \\ ArgS_2 = arctg\left(\dfrac{\left[\sqrt{I_{90}(r_1)I_{90}(r_2)}\sin(\delta_2 - \delta_1)\right]}{\left[\sqrt{I_0(r_1)I_0(r_2)} - \sqrt{I_{90}(r_1)I_{90}(r_2)}\cos(\delta_2 - \delta_1)\right]}\right). \end{cases} \quad (4)$$

$$\begin{cases} |S_3| = \sqrt{\left[\sqrt{I_0(r_1)I_{90}(r_2)}\cos\delta_2 + \sqrt{I_0(r_2)I_{90}(r_1)}\cos\delta_1\right]^2 + \\ +\left[\sqrt{I_0(r_1)I_{90}(r_2)}\sin\delta_2 - \sqrt{I_0(r_2)I_{90}(r_1)}\sin\delta_1\right]^2}; \\ ArgS_3 = arctg\left(\dfrac{\left[\sqrt{I_0(r_1)I_{90}(r_2)}\sin\delta_2 - \sqrt{I_0(r_2)I_{90}(r_1)}\sin\delta_1\right]}{\left[\sqrt{I_0(r_1)I_{90}(r_2)}\cos\delta_2 + \sqrt{I_0(r_2)I_{90}(r_1)}\cos\delta_1\right]}\right). \end{cases} \quad (5)$$

$$\begin{cases} |S_4| = \sqrt{\left[\sqrt{I_0(r_2)I_{90}(r_1)}\sin\delta_1 + \sqrt{I_0(r_1)I_{90}(r_2)}\sin\delta_2\right]^2 + \\ +\left[\sqrt{I_0(r_2)I_{90}(r_1)}\cos\delta_2 + \sqrt{I_0(r_1)I_{90}(r_2)}\cos\delta_1\right]^2}; \\ ArgS_4 = arctg\left(\dfrac{\left[\sqrt{I_0(r_2)I_{90}(r_1)}\cos\delta_2 + \sqrt{I_0(r_1)I_{90}(r_2)}\cos\delta_1\right]}{\left[\sqrt{I_0(r_2)I_{90}(r_1)}\sin\delta_1 + \sqrt{I_0(r_1)I_{90}(r_2)}\sin\delta_2\right]}\right). \end{cases} \quad (6)$$

$$\delta(r) = arctg\left[\left(\frac{S_4(r)S_2(r)}{S_3(r)}\right)\left(\frac{1+\dfrac{I_{90}(r)}{I_0(r)}}{1-\dfrac{I_{90}(r)}{I_0(r)}}\right)\right]. \quad (7)$$

Here I_0 and I_{90} are the intensities in the orientation of the transmission plane of the polarizer 0^0 and 90^0; δ_i - phase shifts between the orthogonal components of the amplitude of the laser radiation at points with coordinates r_1 and r_2.

4. Analysis and discussion of experimental results

The results of SCS - mapping of the distribution of module $\mathrm{Re}\left(S_{i=3;4}(\Delta x;\Delta y)\right)$ and phase $Arg\left(S_{i=3;4}(\Delta x;\Delta y)\right)$ values are presented, which characterize the correlation consistency between the polarization states of the points of microscopic images of histological sections of organs of rats with diabetes:

- kidney tissue - a structured tissue with an optically anisotropic birefringent collagen network;
- spleen tissue - parenchymal tissue with disordered optically anisotropic "islands".

4.1. Maps of the module and phase of the SCS of polarization-heterogeneous images of histological sections of a rat kidney

In fig. 1 and fig. 2 shown SCS - maps of the distribution of module values $S_{i=3}(\Delta x;\Delta y)$ and $S_{i=4}(\Delta x;\Delta y)$ microscopic images of histological sections of the kidney of a healthy and diabetic rat (11 days)

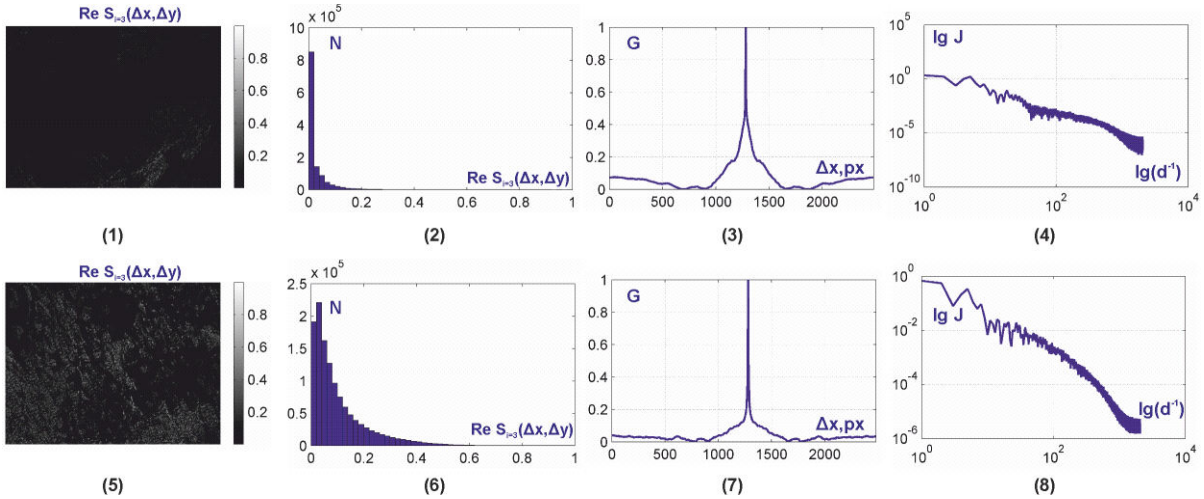

Fig. 1. Maps (coordinate distributions (1), (5), histograms (2), (6), autocorrelation functions (3), (7), logarithmic dependences of power spectra (4), (8)) of an SCS module $\mathrm{Re}\left(S_{i=3}\left(\Delta x;\Delta y\right)\right)$ of polarization-inhomogeneous images of histological sections of a healthy ((1) - (4)) and pathologically altered ((5) - (8)) kidney of a rat.

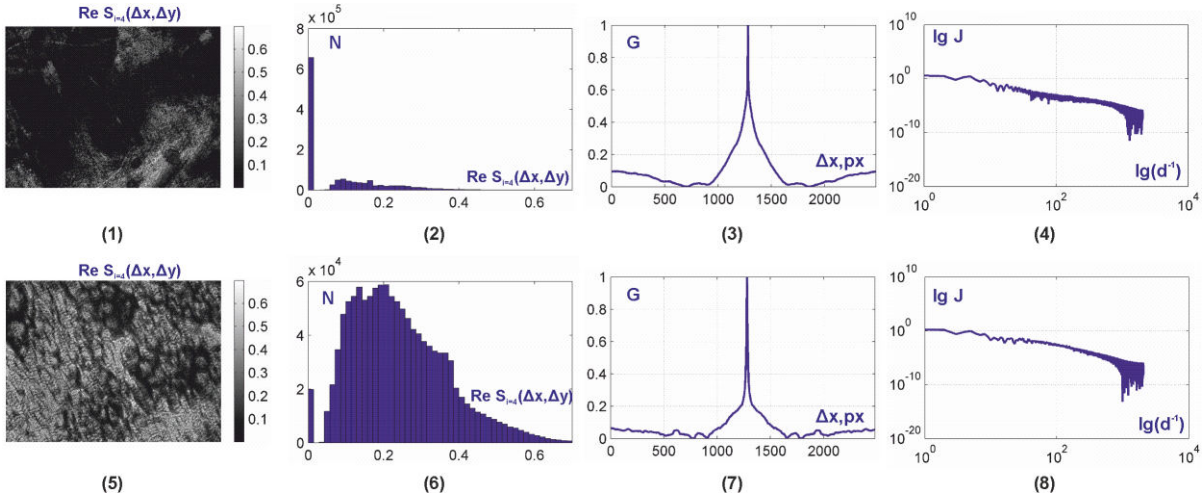

Fig. 2. Maps (coordinate distributions (1), (5), histograms (2), (6), autocorrelation functions (3), (7), logarithmic dependences of power spectra (4), (8)) of an SCS module $\mathrm{Re}\left(S_{i=4}\left(\Delta x;\Delta y\right)\right)$ of polarization-inhomogeneous images of histological sections of a healthy ((1) - (4)) and pathologically altered ((5) - (8)) kidney of a rat.

In fig. 3 and fig. 4 shown the SCS - maps of the distribution of phase values $S_{i=3}\left(\Delta x;\Delta y\right)$ and $S_{i=4}\left(\Delta x;\Delta y\right)$ microscopic images of histological sections of a kidney from a healthy and diabetic rat (11 days)

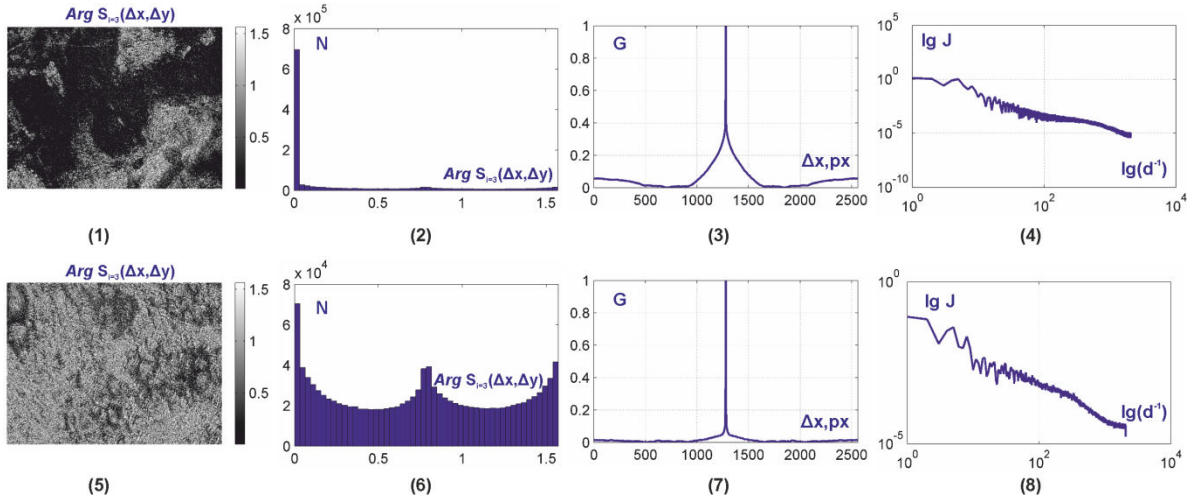

Fig. 3. Maps (coordinate distributions (1), (5), histograms (2), (6), autocorrelation functions (3), (7), logarithmic dependences of power spectra (4), (8)) SCS phases $Arg\left(S_{i=3}\left(\Delta x;\Delta y\right)\right)$ of polarization-inhomogeneous images of histological sections of a healthy ((1) - (4)) and pathologically altered ((5) - (8)) kidney of a rat.

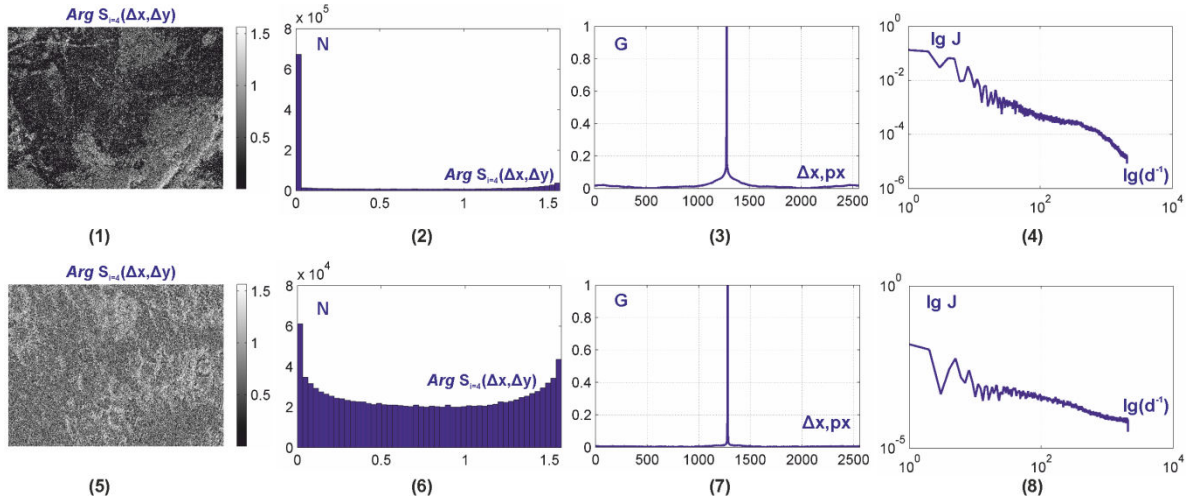

Fig. 4. Maps (coordinate distributions (1), (5), histograms (2), (6), autocorrelation functions (3), (7), logarithmic dependences of power spectra (4), (8)) SCS phases $Arg\left(S_{i=4}\left(\Delta x;\Delta y\right)\right)$ of polarization-inhomogeneous images of histological sections of a healthy ((1) - (4)) and pathologically altered ((5) - (8)) kidney of a rat.

A comparative analysis[21-26] of the structure of maps of the SCS module $\mathrm{Re}\left(S_{i=3;4}\left(\Delta x;\Delta y\right)\right)$ of polarization-inhomogeneous fields of rat kidney samples of both types revealed an increase in the correlation consistency of polarization states in the image of the sample with diabetes. This is indicated analytically:

• the average and half-widths of the histograms $N^{*}\left(\mathrm{Re}\left(S_{i=3;4}\left(\Delta x;\Delta y\right)\right)\right)$ of the distribution of the values of the boundary field module $\mathrm{Re}\left(S_{i=3;4}\left(\Delta x;\Delta y\right)\right)$ of the histological section of the kidney of a rat with diabetes mellitus are growing (fig. 1, fig. 2, fragments (2), (6));

• similar changes take place for the values of statistical moments of the 1st and 2nd orders characterizing the distribution of the SCS phase $Arg\left(S_{i=3;4}\left(\Delta x;\Delta y\right)\right)$ values of the polarization-inhomogeneous image of the histological section of the kidney of a diabetic rat (fig. 3, fig. 4, fragments (2), (6));

• statistical moments of higher orders characterizing the asymmetry and excess of the distributions of the module and phase of the SCS images of a patient's kidney sample change according to the following scenario $\begin{cases} Z_3\left(\mathrm{Re}\left(S_{i=3;4}(\Delta x;\Delta y)\right);Arg\left(S_{i=3;4}(\Delta x;\Delta y)\right)\right)\downarrow; \\ Z_4\left(\mathrm{Re}\left(S_{i=3;4}(\Delta x;\Delta y)\right);Arg\left(S_{i=3;4}(\Delta x;\Delta y)\right)\right)\downarrow. \end{cases}$;

• autocorrelation dependences of the coordinate distributions of the module and the SCS phase are characterized by an increase in half width and a decrease in peak sharpness $\begin{cases} Z_2^K\left(\mathrm{Re}\left(S_{i=3;4}(\Delta x;\Delta y)\right);Arg\left(S_{i=3;4}(\Delta x;\Delta y)\right)\right)\uparrow; \\ Z_4^K\left(\mathrm{Re}\left(S_{i=3;4}(\Delta x;\Delta y)\right);Arg\left(S_{i=3;4}(\Delta x;\Delta y)\right)\right)\downarrow. \end{cases}$

Quantitatively, the possibility of Stokes-correlometric differentiation of two groups of samples (36 histological sections each) of the kidney is illustrated by the data shown in table 1 and table 2.

Table1. Statistical, correlation and fractal parameters of the SKS module maps of polarization-heterogeneous images of histological sections of a healthy and pathologically altered rat kidney

Parameters	$\mathrm{Re}\left(S_{i=3}(\Delta x;\Delta y)\right)$		$\mathrm{Re}\left(S_{i=4}(\Delta x;\Delta y)\right)$	
State	Norm	Diabetes	Norm	Diabetes
Z_1	$0{,}016 \pm 0{,}0011$	$0{,}027 \pm 0{,}0019$	$0{,}041 \pm 0{,}0034$	$0{,}14 \pm 0{,}011$
Z_2	$0{,}007 \pm 0{,}0005$	$0{,}013 \pm 0{,}0011$	$0{,}011 \pm 0{,}009$	$0{,}23 \pm 0{,}016$
Z_3	$3{,}78 \pm 0{,}24$	$1{,}35 \pm 0{,}12$	$2{,}07 \pm 0{,}19$	$0{,}69 \pm 0{,}055$
Z_4	$23{,}18 \pm 1{,}39$	$6{,}24 \pm 0{,}54$	$3{,}95 \pm 0{,}22$	$0{,}82 \pm 0{,}069$
Z_2^k	$0{,}11 \pm 0{,}009$	$0{,}07 \pm 0{,}005$	$0{,}09 \pm 0{,}007$	$0{,}06 \pm 0{,}005$
Z_4^k	$0{,}98 \pm 0{,}078$	$2{,}48 \pm 0{,}16$	$0{,}87 \pm 0{,}068$	$1{,}63 \pm 0{,}12$
D^f	$0{,}17 \pm 0{,}013$	$0{,}22 \pm 0{,}017$	$0{,}21 \pm 0{,}017$	$0{,}32 \pm 0{,}021$

Table 2. Statistical, correlation and fractal parameters of the SKS module maps of polarization-heterogeneous images of histological sections of a healthy and pathologically altered rat kidney

Parameters	$Arg\left(S_{i=3}(\Delta x;\Delta y)\right)$		$Arg\left(S_{i=4}(\Delta x;\Delta y)\right)$	
State	Norm	Diabetes	Norm	Diabetes
Z_1	$0{,}012 \pm 0{,}001$	$0{,}18 \pm 0{,}013$	$0{,}01 \pm 0{,}001$	$0{,}15 \pm 0{,}012$
Z_2	$0{,}016 \pm 0{,}0012$	$0{,}22 \pm 0{,}017$	$0{,}014 \pm 0{,}0011$	$0{,}2 \pm 0{,}015$
Z_3	$1{,}95 \pm 0{,}13$	$0{,}64 \pm 0{,}054$	$1{,}79 \pm 0{,}14$	$0{,}56 \pm 0{,}043$
Z_4	$4{,}09 \pm 0{,}33$	$0{,}78 \pm 0{,}061$	$3{,}29 \pm 0{,}27$	$0{,}67 \pm 0{,}051$
Z_2^k	$0{,}1 \pm 0{,}009$	$0{,}06 \pm 0{,}005$	$0{,}07 \pm 0{,}007$	$0{,}05 \pm 0{,}005$
Z_4^k	$1{,}48 \pm 0{,}078$	$3{,}64 \pm 0{,}16$	$2{,}37 \pm 0{,}068$	$4{,}61 \pm 0{,}12$
D^f	$0{,}15 \pm 0{,}013$	$0{,}21 \pm 0{,}017$	$0{,}24 \pm 0{,}017$	$0{,}27 \pm 0{,}021$

The most sensitive indicators are highlighted in tables 1 and 2 in gray.

4.2. Maps of the module and phase of the SCS of polarization-heterogeneous images of histological sections of rat liver

In fig. 5 and fig. Figure 6 shown SCS - maps of the distribution of module values $\mathrm{Re}\left(S_{i=3}(\Delta x;\Delta y)\right)$ and $\mathrm{Re}\left(S_{i=4}(\Delta x;\Delta y)\right)$ microscopic images of histological sections of the parenchymal tissue of the liver of a healthy and diabetic rat (11 days).

In fig. 7 and fig. 8 shown the SCS - maps of the distribution of phase values $S_{i=3}(\Delta x;\Delta y)$ and $S_{i=4}(\Delta x;\Delta y)$ microscopic images of histological sections of the liver of a healthy and diabetic rat (11 days).

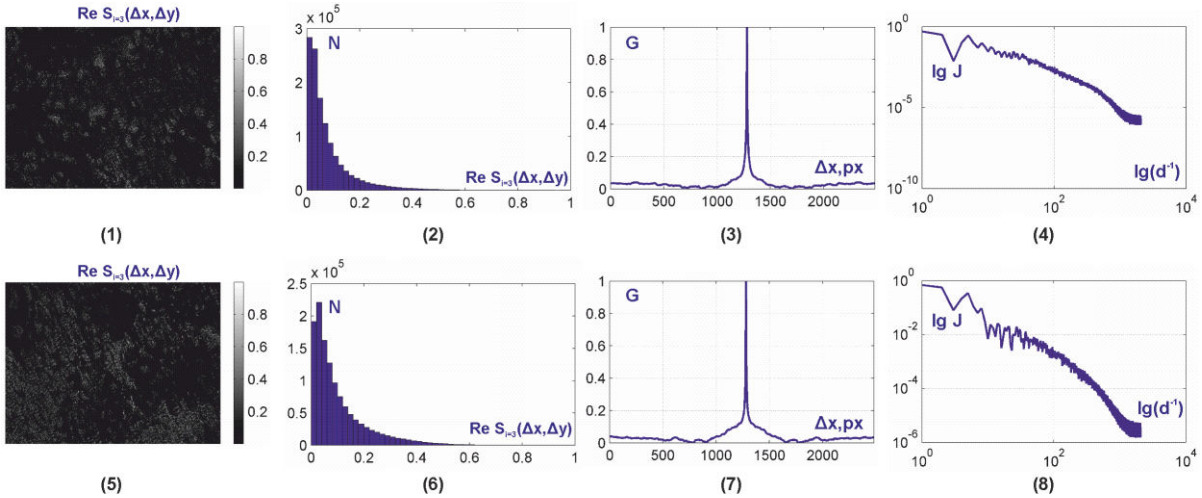

Fig. 5. Maps (coordinate distributions (1), (5), histograms (2), (6), autocorrelation functions (3), (7), logarithmic dependences of power spectra (4), (8)) of an SCS module $\mathrm{Re}(S_{i=3}(\Delta x;\Delta y))$ of polarization-inhomogeneous images of histological sections of a healthy ((1) - (4)) and pathologically altered ((5) - (8)) liver of a rat.

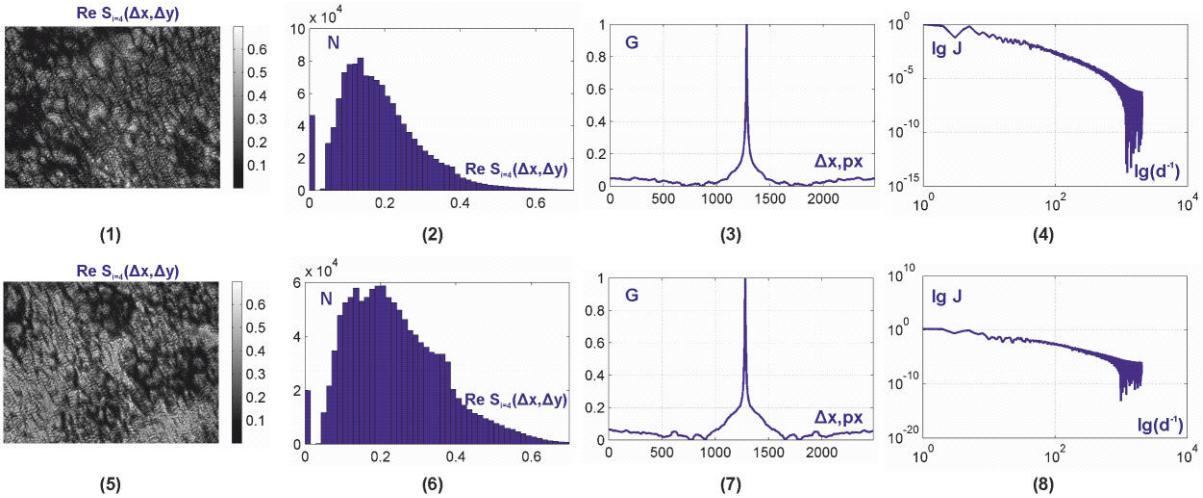

Fig. 6. Maps (coordinate distributions (1), (5), histograms (2), (6), autocorrelation functions (3), (7), logarithmic dependences of power spectra (4), (8)) of an SCS module $\mathrm{Re}(S_{i=4}(\Delta x;\Delta y))$ of polarization-inhomogeneous images of histological sections of a healthy ((1) - (4)) and pathologically altered ((5) - (8)) liver of a rat.

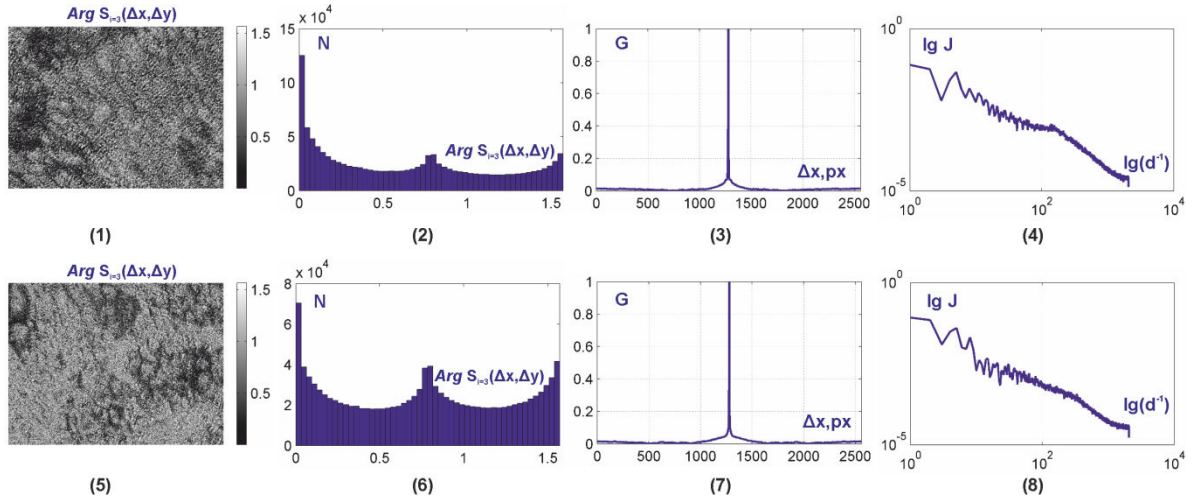

Fig. 7. Maps (coordinate distributions (1), (5), histograms (2), (6), autocorrelation functions (3), (7), logarithmic dependences of power spectra (4), (8)) SCS phases $Arg\left(S_{i=3}(\Delta x;\Delta y)\right)$ of polarization-inhomogeneous images of histological sections of a healthy ((1) - (4)) and pathologically altered ((5) - (8)) liver of a rat.

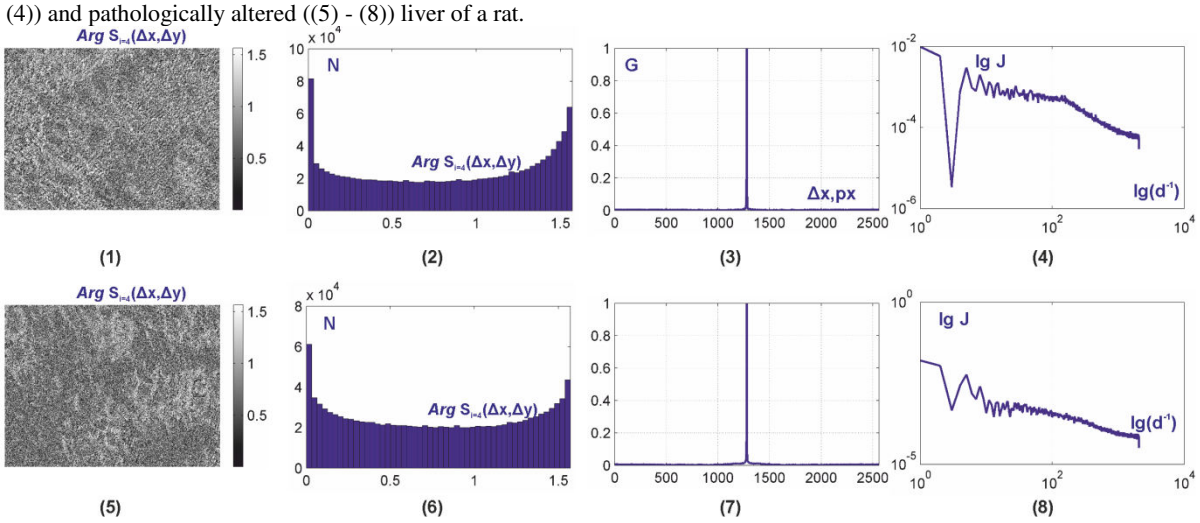

Fig. 8. Maps (coordinate distributions (1), (5), histograms (2), (6), autocorrelation functions (3), (7), logarithmic dependences of power spectra (4), (8)) SCS phases $Arg\left(S_{i=4}(\Delta x;\Delta y)\right)$ of polarization-inhomogeneous images of histological sections of a healthy ((1) - (4)) and pathologically altered ((5) - (8)) liver of a rat.

A comparative analysis (table 3 and table 4) of the structure maps of the module $\mathrm{Re}\left(S_{i=3;4}(\Delta x;\Delta y)\right)$ and the SCS phase $Arg\left(S_{i=3;4}(\Delta x;\Delta y)\right)$ of polarization-inhomogeneous fields of rat liver samples of both types was found

$$\begin{cases} Z_1\left(\mathrm{Re}\left(S_{i=3;4}(\Delta x;\Delta y)\right);Arg\left(S_{i=3;4}(\Delta x;\Delta y)\right)\right)\uparrow; \\ Z_2\left(\mathrm{Re}\left(S_{i=3;4}(\Delta x;\Delta y)\right);Arg\left(S_{i=3;4}(\Delta x;\Delta y)\right)\right)\uparrow. \end{cases} \begin{cases} Z_3\left(\mathrm{Re}\left(S_{i=3;4}(\Delta x;\Delta y)\right);Arg\left(S_{i=3;4}(\Delta x;\Delta y)\right)\right)\downarrow; \\ Z_4\left(\mathrm{Re}\left(S_{i=3;4}(\Delta x;\Delta y)\right);Arg\left(S_{i=3;4}(\Delta x;\Delta y)\right)\right)\downarrow. \end{cases}$$

$$\begin{cases} Z_2^K\left(\mathrm{Re}\left(S_{i=3;4}(\Delta x;\Delta y)\right);Arg\left(S_{i=3;4}(\Delta x;\Delta y)\right)\right)\uparrow; \\ Z_4^K\left(\mathrm{Re}\left(S_{i=3;4}(\Delta x;\Delta y)\right);Arg\left(S_{i=3;4}(\Delta x;\Delta y)\right)\right)\downarrow. \end{cases}$$

Table 3 A comparative analysis (table 3 and table 4) of the structure maps of the module $\mathrm{Re}\left(S_{i=3;4}(\Delta x;\Delta y)\right)$ and the SCS phase $Arg\left(S_{i=3;4}(\Delta x;\Delta y)\right)$ of polarization-inhomogeneous fields of rat liver samples

Parameters	$Arg\left(S_{i=3}(\Delta x;\Delta y)\right)$		$Arg\left(S_{i=4}(\Delta x;\Delta y)\right)$	
State	Norm	Diabetes	State	Norm
Z_1	$0{,}018 \pm 0{,}0012$	$0{,}023 \pm 0{,}0017$	$0{,}11 \pm 0{,}093$	$0{,}15 \pm 0{,}012$
Z_2	$0{,}009 \pm 0{,}0005$	$0{,}015 \pm 0{,}0012$	$0{,}12 \pm 0{,}09$	$0{,}21 \pm 0{,}016$
Z_3	$3{,}27 \pm 0{,}22$	$2{,}15 \pm 0{,}17$	$1{,}07 \pm 0{,}11$	$0{,}89 \pm 0{,}065$
Z_4	$5{,}12 \pm 0{,}39$	$2{,}24 \pm 0{,}14$	$0{,}95 \pm 0{,}072$	$0{,}62 \pm 0{,}049$
Z_2^k	$0{,}11 \pm 0{,}009$	$0{,}08 \pm 0{,}005$	$0{,}095 \pm 0{,}007$	$0{,}067 \pm 0{,}005$
Z_4^k	$1{,}08 \pm 0{,}088$	$1{,}84 \pm 0{,}16$	$0{,}89 \pm 0{,}069$	$1{,}36 \pm 0{,}11$
D^f	$0{,}19 \pm 0{,}015$	$0{,}27 \pm 0{,}019$	$0{,}22 \pm 0{,}016$	$0{,}31 \pm 0{,}023$

Table4 A comparative analysis (table 3 and table 4) of the structure maps of the module $\mathrm{Re}\left(S_{i=3;4}(\Delta x;\Delta y)\right)$ and the SCS phase $Arg\left(S_{i=3;4}(\Delta x;\Delta y)\right)$ of polarization-inhomogeneous fields of rat liver samples

Parameters	$Arg\left(S_{i=3}(\Delta x;\Delta y)\right)$		$Arg\left(S_{i=4}(\Delta x;\Delta y)\right)$	
State	Norm	Diabetes	State	Norm
Z_1	$0{,}12 \pm 0{,}009$	$0{,}17 \pm 0{,}014$	$0{,}14 \pm 0{,}011$	$0{,}22 \pm 0{,}017$
Z_2	$0{,}16 \pm 0{,}012$	$0{,}22 \pm 0{,}017$	$0{,}14 \pm 0{,}011$	$0{,}21 \pm 0{,}015$
Z_3	$0{,}91 \pm 0{,}082$	$0{,}63 \pm 0{,}057$	$0{,}77 \pm 0{,}064$	$0{,}58 \pm 0{,}041$
Z_4	$1{,}09 \pm 0{,}13$	$0{,}71 \pm 0{,}061$	$1{,}29 \pm 0{,}12$	$0{,}63 \pm 0{,}051$
Z_2^k	$0{,}11 \pm 0{,}01$	$0{,}07 \pm 0{,}006$	$0{,}08 \pm 0{,}007$	$0{,}06 \pm 0{,}005$
Z_4^k	$1{,}78 \pm 0{,}18$	$2{,}86 \pm 0{,}26$	$2{,}67 \pm 0{,}22$	$3{,}71 \pm 0{,}31$
D^f	$0{,}17 \pm 0{,}013$	$0{,}26 \pm 0{,}019$	$0{,}18 \pm 0{,}017$	$0{,}29 \pm 0{,}023$

The most sensitive indicators are highlighted in tables 3 and 4 in gray.

If we compare the diagnostic data of the statistical, correlation, and fractal analysis of the maps of the module and the SCS phase of polarization-heterogeneous images of structured (kidney) and parenchymal (spleen) rat tissues, then we can state:

• high sensitivity to changes in the optical anisotropy of structured fibrillar networks — differences between the values of objective parameters reach the same order of magnitude;

• high sensitivity to changes in the optical anisotropy of island parenchymal structures - differences between the values of objective parameters reach 2 times.

5. Social aspects of application of diagnostic methods

The problem of detecting and diagnosing both prevention of general and occupational diseases of workers is quite a problem throughout the continental dimension. Therefore, the issue of early detection and diagnosis of various kinds of diseases, especially among the working population, is an important aspect of the social well-being of society and the state.

Detection and early diagnosis of workers 'diseases makes it possible to assess their health status, to identify diseases that can aggravate even more when exposed to harmful production factors at the enterprise or organization and may be contraindications for further transfer to another job.

The purpose of early diagnosis of workers' diseases is to dynamically monitor their health under the influence of harmful production factors, prevention and timely establishment of the initial signs of various kinds of diseases that may

impede the continuation of work in the relevant profession, qualifications. Such early diagnosis helps to identify cardiovascular, oncological diseases, diabetes mellitus, musculoskeletal system (etc.) and the appointment of preventive treatment courses, individual therapeutic and preventive measures, as well as addressing the issue of further employment with the development of a set of measures to reduce the incidence and prevention of various diseases of workers. The main task of early diagnosis of workers' diseases is to conduct medical and health-improving and preventive measures with the aim of rational employment, taking into account their state of health.

Additional arguments for the introduction of early diagnosis of employee diseases is the fact that allows you to assess the health status of the employee, to identify the time of onset of the initial signs of the disease, which have not yet caused the transfer or dismissal of him from work. As a result of such a diagnosis, information about the increased frequency of a given disease in a given enterprise or structural unit may be useful.

The early diagnosis of workers' diseases is directly related to the concept of human development and the concept of decent work, which provides for the work of women and men in conditions of equality, freedom, security and human dignity. It covers job opportunities that are productive and bring fair income, ensure workplace safety and provide social protection for workers. To this end, the collective agreement should reflect the main aspects of the concept of decent work: creating an atmosphere conducive to effective work, increasing labor efficiency based on the safety of each workplace and preserving the life and health of the employee in the labor process.

CONCLUSION

1. For the first time by the method of Stokes-correlometric mapping, the physical processes of changes in optical anisotropy (distribution of optical axis directions and phase modulation) of biological structured (kidney) and parenchymal (liver) tissues of rat internal organs, which are caused by systemic pathology (diabetes), were identified and analyzed as part of a statistical analysis.

2. The most sensitive parameters (statistical moments of the 1st – 4th orders of magnitude, the correlation moment of the 4th order) to changes in the distribution structure of the magnitude and phase of the SCS of the 3rd and 4th parameters of the "two-point" parameter of the Stokes polarization heterogeneous microscopic images of histological sections of healthy and diabetic rat kidney and liver tissues. On this basis, the method of Stokes-correlometric mapping is used to differentiate the changes in the optical anisotropy of such samples with good balanced accuracy, the accuracy of direct polarization mapping methods is 20% to 30% higher, namely:

- ModuleSCS - $84\% \le \max Ac \le 90\%$,.
- PhaseSCS - $80\% \le \max Ac \le 86\%$.

3. Some social and legal aspects of implementation of the developed biophysical methods of early diagnostics in the public environment are considered

REFERENCES

[1]. Wang X. Propagation of polarized light in birefringent turbid media: a Monte Carlo study / X. Wang, L.-H. Wang // J. Biomed. Opt. – 2002. – Vol. 7. – P. 279-290.

[2]. Tuchin V. V. Handbook of optical biomedical diagnostics / V. V. Tuchin. – Bellingham : SPIE Press, 2002. – 1110 p.

[3]. Yao G. Two-dimensional depth-resolved Mueller matrix characterization of biological tissue by optical coherence tomography / G. Yao, L. V. Wang // Opt. Lett. – 1999. – V. 24. – P. 537-539.

[4]. Tower T. T. Alignment Maps of Tissues: I. Microscopic Elliptical Polarimetry / T. T. Tower, R. T. Tranquillo // Biophys. J. – 2001. – Vol. 81. – P. 2954-2963.

[5]. Lu S. Interpretation of Mueller matrices based on polar decomposition / S. Lu, R. A. Chipman // J. Opt. Soc. Am. A. – 1996. – Vol. 13. – P.1106-1113.

[6]. Ghosh Nirmalya. Techniques for fast and sensitive measurements of two-dimensional birefringence distributions / Nirmalya Ghosh, I. Alex Vitkin // Journal of Biomedical Optics. – 2011. – № 16(11). – P. 110801.

[7]. V. V. Tuchin, L. Wang, and D. A` . Zimnyakov, Optical Polarization in Biomedical Applications, New York, USA (2006).

[8]. Angelsky, O.V., Hanson, S.G., Maksimyak, P.P., Maksimyak, A.P., Zenkova, C.Yu., Polyanskii, P.V., Ivanskyi, D.I., "Influence of evanescent wave on birefringent microplates," (2017) Optics Express, 25 (3), pp. 2299-2311.

[9]. 2. Angelsky, O.V., Ushenko, Y.A., Dubolazov, A.V., Telenha, O.Yu., "The interconnection between the coordinate distribution of mueller-matrixes images characteristic values of biological liquid crystals net and the pathological changes of human tissues,"(2010) Advances in Optical Technologies, art. no. 130659.

[10]. Bekshaev, A.Ya., Angelsky, O.V., Sviridova, S.V., Zenkova, C.Yu., "Mechanical action of inhomogeneously polarized optical fields and detection of the internal energy flows," (2011) Advances in Optical Technologies, art. no. 723901.

[11]. Angelsky, O.V., Maksimyak, P.P., Perun, T.O., “Optical correlation method for measuring spatial complexity in optical fields,” (1993) Optics Letters, 18 (2), pp. 90-92.
[12]. Angelsky, O.V., Ushenko, A.G., Ushenko, Y.A., Pishak, V.P., “Statistical and fractal structure of biological tissue mueller matrix images,” (2007) Optical Correlation Techniques and Applications, pp. 213-265.
[13]. Angelsky, O.V., Ushenko, A.G., Pishak, V.P., Burkovets, D.N., Yermolenko, S.B., Pishak, O.V., Ushenko, Yu.A., “Coherent introscopy of phase-inhomogeneous surfaces and layers,” (2000) Proceedings of SPIE - The International Society for Optical Engineering, 4016, pp. 413-418.
[14]. Angelsky, O.V., “Optical correlation techniques and applications,”(2007) Optical Correlation Techniques and Applications, pp. 1-270.
[15]. Angelsky, O.V., Maksimyak, P.P., “Optical diagnostics of slightly rough surfaces,” (1992) Applied Optics, 31 (1), pp. 140-143.
[16]. Angelsky, O.V., Maksimyak, P.P., “Polarization-interference measurement of phase-inhomogeneous objects,” (1992) Applied Optics, 31 (22), pp. 4417-4419.
[17]. Angelsky, O. V., Bekshaev, A. Ya., Maksimyak, P. P., Maksimyak, A. P., Hanson, Steen Grüner, “ Low-temperature laser-stimulated controllable generation of micro-bubbles in a water suspension of absorptive colloid particles,” Optics Express (2018), Vol. 26, No. 11. pp. 13995-14009.
[18]. Ushenko, Yu.A., Tomka, Yu.Ya., Dubolazov, A.V., Telen'ga, O.Yu. Diagnostics of optical anisotropy changes in biological tissues using Müller matrix (2011) Quantum Electronics, 41 (3), pp. 273-277.
[19]. Ushenko, Yu.A., Tomka, Yu.Ya., Dubolazov, A.V. Laser diagnostics of anisotropy in birefringent networks of biological tissues in different physiological conditions (2011) Quantum Electronics, 41 (2), pp. 170-175.
[20]. Ushenko, Y.A., Dubolazov, O.V., Karachevtsev, A.O. Statistical structure of skin derma Mueller matrix images in the process of cancer changes (2011) Optical Memory and Neural Networks (Information Optics), 20 (2), pp. 145-154.
[21]. Ushenko, V.A., Dubolazov, A.V. Correlation and self similarity structure of polycrystalline network biological layers mueller matrices images (2013) Proceedings of SPIE - The International Society for Optical Engineering, 8856, 88562D.
[22]. Ushenko, A.G., Dubolazov, A.V., Ushenko, V.A., Novakovskaya, O.Y. Statistical analysis of polarization-inhomogeneous Fourier spectra of laser radiation scattered by human skin in the tasks of differentiation of benign and malignant formations (2016) Journal of Biomedical Optics, 21 (7), 071110.
[23]. Ushenko, Y.A., Dubolazov, A.V., Angelsky, A.P., Sidor, M.I., Bodnar, G.B., Koval, G., Zabolotna, N.I., Smolarz, A., Junisbekov, M.S. Laser polarization fluorescence of the networks of optically anisotropic biological crystals (2013) Proceedings of SPIE - The International Society for Optical Engineering, 8698, 869809.
[24]. Ushenko, Yu.A., Bachynsky, V.T., Vanchulyak, O.Ya., Dubolazov, A.V., Garazdyuk, M.S., Ushenko, V.A. Jones-matrix mapping of complex degree of mutual anisotropy of birefringent protein networks during the differentiation of myocardium necrotic changes (2016) Applied Optics, 55 (12), pp. B113-B119.
[25]. Angelsky, O. V., Yermolenko, S. B., Prydij, O., Ushenko, A. G., Ushenko, Y. A., & Ushenko, Y. G., “Polarization-interference structure of speckle fields of the rough skin surface,” Journal of Holography and Speckle 3(1), 27-34 (2006).
[26]. V. A. Ushenko, N. I. Zabolotna, S. V. Pavlov, D. M. Burcovets, O. Yu. Novakovska, Olexander V. Dubolazov, "Mueller-matrices polarization selection of two-dimensional linear and circular birefringence images," Proc. SPIE 9066, Eleventh International Conference on Correlation Optics, 90661X (17 December 2013).